Transport of moderately sorted gravel at low bed shear stresses: The role of fine sediment infiltration

E. Perret, Céline Berni, B. Camenen, A. Herrero, K. El Kadi Abderrezzak

Author-produced version of the article published in Earth Surface Processes and Landforms , 2018
The original publication is available at https://onlinelibrary.wiley.com/doi/abs/10.1002/esp.4322
doi : 10.1002/esp.4322

Transport of moderately sorted gravel at low bed shear stresses: the role of fine sediment infiltration

E. Perret[1*], C. Berni[1], B. Camenen[1], A. Herrero[1,2], and K. El Kadi Abderrezzak[3]

[1]Irstea, UR HHLY, centre de Lyon-Villeurbanne, 5 rue de la Doua, CS20244, F-69625 Villeurbanne Cedex, France
[2]Now at Catalan Institute for Water Research, 101 Carrer Emili Grahit, 17003, Girona, Spain
[3]EDF R&D, LNHE / LHSV, 6 Quai Watier, F-78401 Chatou, France
[*]Corresponding author, e-mail: emeline.perret@irstea.fr

May 24, 2018

Abstract

A reliable estimation of sediment transport in gravel-bed streams is important for various practical engineering and biological studies (e.g., channel stability design, bed degradation/aggradation, restoration of spawning habitat). In the present work, we report original laboratory experiments investigating the transport of gravel particles at low bed shear stresses. The laboratory tests were conducted under unsteady flow conditions inducing low bed shear stresses, with detailed monitoring of the bed topography using a laser scanner. Effects of bed surface arrangements were documented by testing loose and packed bed configurations. Effects of fine sediments were examined by testing beds with sand, artificial fine sand or cohesive silt infiltrated in the gravel matrix. Analysis of the experimental data revealed that the transport of gravel particles depends upon the bed arrangement, the bed material properties (e.g., size and shape, consolidation index, permeability) and the concentration of fine sediments within the surface layer of moving grains. This concentration is directly related to the distribution of fine particles within the gravel matrix (i.e., bottom-up infiltration or bridging) and

their transport mode (i.e., bedload or suspended load). Compared to loose beds, the mobility of gravel is reduced for packed beds and for beds clogged from the bottom up with cohesive fine sediments; in both cases, the bed shear stress for gravel entrainment increases by about 12 %. On the other hand, the mobility of gravel increases significantly (bed shear stress for particle motion decreasing up to 40 %) for beds clogged at the surface by non-cohesive sand particles.

Keywords: sediment transport; fine sediment clogging; bed arrangement; incipient motion; laboratory experiments.

Introduction

A mountain river is a dynamic system. Its flow and bed morphology change due to natural events (e.g., changes in flow conditions and sediment supply) or human activities, resulting in overbank floods, structure failure and fish stock variability (Pitlick and Van Steeter, 1998). Mountain rivers are often formed with grain sizes ranging from clay to pebble (diameters between micrometers and decimeters), which leads to selective sediment transport, fine-coarse particle interactions, infiltration and clogging of fine sediments within the gravel substrate. The amount and type of fine sediment found in coarse substrate can have implications for the bed morphology dynamics, the health of aquatic biota, surface-groundwater interactions as well as water quality (Kondolf and Wolman, 1993; Wharton et al., 2017).

In gravel-bed streams, partial transport induced by low-flow conditions is more frequent than full mobility (all grain sizes are mobile, the bed surface completely disrupted due to high flow conditions). Therefore, the bedload rate can be highly variable in time and space because the entrainment threshold is only slightly exceeded (Wilcock and McArdell, 1993). In this context, quantitative estimates of the threshold conditions for particle motion and of gravel bedload at low shear stresses are difficult (Buffington and Montgomery, 1997). The use of the Shields diagram or bedload formulae based on excess bed shear stress, originally developed for non-cohesive and well-sorted bed materials, is questionable (Wilcock, 2001; Parker,

2008). Most of these formulae do no take into account aspects such as: the Grain Size Distribution (GSD) of bed material; the specific conditions for incipient motion of each grain-size fraction (Proffitt and Sutherland, 1983); and the role played by surface bed structures, specifically grain arrangement and orientation (Voepel et al., 2017), and by fine sediments mortaring the gravel on bed mobility (Hodge et al., 2013; Wainwright et al., 2015).

For poorly (and moderately) sorted gravel materials, the formation of a surface armor layer is generally observed under steady flow and no sediment feeding conditions (Church et al., 1998; Guney et al., 2013), which implies a bed surface coarsening (Hassan and Church, 2000), an increase in grain imbrication (Mao et al., 2011; Qin et al., 2012), and the formation of grain patterns (e.g. clusters, microforms; Marion et al., 2003; Curran, 2010). Under unsteady flows, Mao (2012) and Guney et al. (2013) highlighted significant changes in gravel bed surface organization due to the antecedent flow history and the initial degree of bed armoring and arrangement. The arrangement of the bed surface was identified as an important factor affecting gravel mobility, but its effect was not quantified. The transport of bimodal material formed with sand and gravel mixture was examined mainly in laboratory conditions (e.g. Ikeda and Iseya, 1988; Wilcock and Crowe, 2003; Curran and Wilcock, 2005), with the aim of developing empirical formulae for the computation of bedload. Increasing sand content, the bed becomes sand-dominant with gravel particles moving individually over a surface sand layer (Wilcock et al., 2001). Wilcock and Kenworthy (2002) developed a two-fraction model for sand-gravel mixture transport. Wilcock and Crowe (2003) proposed a surface-based transport model for mixed-size sediments considering the hiding/exposure effect and the nonlinear effect of sand content.

The process of fine sediment infiltration into immobile clean gravel was investigated, mainly for non-cohesive sediments, experimentally (Einstein, 1968; Beschta and Jackson., 1979; Schälchli, 1992; Haynes et al., 2009; Gibson et al., 2010; Wren et al., 2011, among others) and theoretically (Sakthivadivel and Einstein, 1970; Cui

et al., 2008; Nuñez Gonzalez, 2016; Herrero and Berni, 2016). To a lesser extent, one can find a number of field (Frostick et al., 1984; Lisle, 1989; Sear, 1993) and laboratory experiments examining the infiltration of cohesive sediments (Krishnappan and Engel, 2006). Depending on the fine-to-coarse particle diameter ratio (Gibson et al., 2009), two infiltration mechanisms can occur: 1) deep infiltration of fine sediments down to an impermeable bottom and progressive filling of the gravel pores from the bottom upward (a process called Unimpeded Static Percolation (USP)); 2) trapping of fine grains at the surface pore throats that prevents further fine sediments from infiltrating into the subsurface, therefore forming a surface clogged layer (i.e. bridge or seal). To the author's knowledge, no study describing how the clogged gravel material is mobilized is available. Marquis and Roy (2012) argued that fine sediment infiltration and dynamics may affect gravel bed dilation (i.e., reorganization of coarse particles into a looser packing) and contraction (i.e., tighter packing) during low flood events.

The role of cohesive sediments (silt/clay) on inception of gravel motion was investigated in a few field (Reid et al., 1985; Barzilai et al., 2013) and laboratory studies (Kothyari and Jain, 2008; Jain and Kothyari, 2009). Cohesive particles consolidate the gravel bed, leading to an interlocking bed structure that modifies bedload drastically (Hassan and Church, 2000). Gravel transport decreases with an increase in clay content (Jain and Kothyari, 2009; Barzilai et al., 2013), but depends on various parameters (e.g., clay type and percentage, water content in the cohesive fraction, undrained shear strength, unconfined compressive strength, plasticity index).

The review presented above indicates that a considerable amount of effort has been involved in the investigation of non-cohesive, non-uniform selective sediment transport leading to an armor layer. Similarly, studies examining the infiltration of non-cohesive fines through immobile, well-sorted gravel beds are abundant. However, the transport of gravel at low bed shear stress (i.e., flows generating a very low but measurable bedload) along with considering the role of fine sediments and struc-

tures of the surface bed material has not been examined yet. This is unfortunate, because understanding the factors controlling the gravel mobility at low bed shear stress is required to quantify and model bedload in mountain streams. Indeed, the largest uncertainty in predictive models is observed for this range of low bed shear stresses (Camenen and Larson, 2005; Recking et al., 2012). Our research addresses this gap by quantifying the transport of moderately sorted gravel close to the incipient motion conditions. We report the results from a series of original experiments conducted in a straight laboratory flume under unsteady flow conditions generating low bed shear stresses. Two different bed configurations (loose vs packed) were tested to reflect the role of grain arrangement and orientation on gravel mobility. The effects of fine sediments were examined by infiltrating different types of fine sediments in the gravel matrix.

This paper is organized as follows: after presenting the experimental set-up and describing how the infiltrated and packed beds were created in the laboratory, the results and main observed processes are summarized. Then the main factors affecting gravel transport at low bed shear stresses are discussed; a methodology for improving the computation of bedload in gravel beds is also presented. The last section provides concluding remarks.

Materials and methods

Experimental facility

The sediment transport experiments were carried out in an 18 m-long, 1 m-wide and 0.8 m-deep tilting flume with glass walls (Figure 1). This facility is located in the Irstea's Hydraulic and Hydromorphology Laboratory (HHLab) in Lyon-Villeurbanne (France). The flume longitudinal slope was set at 1 %. An electromagnetic flowmeter (Krohne Optiflux) measured the flow discharge (Q). A honeycomb straightener eliminated flow turbulent structures at the entrance. A 1 m-long weir with adjustable slope and height was placed at the downstream end to control the

Author-produced version of the article published in Earth Surface Processes and Landforms , 2018
The original publication is available at https://onlinelibrary.wiley.com/doi/abs/10.1002/esp.4322
doi : 10.1002/esp.4322

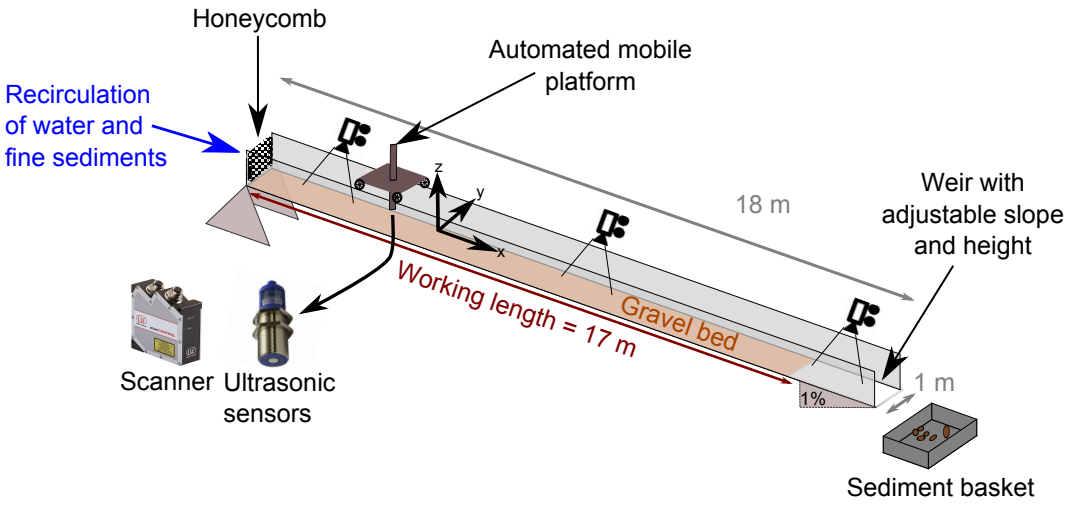

Figure 1: Experimental set-up.

water depth and to achieve a uniform flow condition, without impeding bedload. The flow was qualified as uniform when its free surface was approximately parallel to the longitudinal bed profile. The weir settings were determined after several trials. In our experiments, the flow depth was the same (within ± 1 cm) at every sections of the channel located between 6 and 18 m downstream of the flume inlet. Ultrasonic sensors (Microsonic mic+130/IU/TC) and a laser scanner (scanControl 2900 Micro-Epsilon, vertical resolution: 2 μm), installed on an automated mobile platform, measured the water surface and bed topography, respectively. The analysis of laser scanner surveys provides indicators of bed surface arrangement, such as the geometrical grain roughness of the bed surface (σ_{zg}), lengths of the bed surface structures in the streamwise (Δ_{x0}) and cross-stream direction (Δ_{y0}), the armoring degree (A_r) and the preferential orientation of bed surface grains (Φ) (Marion et al., 2003; Perret et al., 2016). A closed recirculating system supplied clear water or water mixed with fine sediments (grain sizes less than 0.5 mm) into the flume. There was no upstream gravel feeding. Rolling baskets collected the transported gravel at the downstream end of the flume, so that bedload rate measurements could be performed.

The experimental configurations were chosen to be representative of alpine rivers in terms of slope (1 %), Shields numbers ($0.04 \leq \tau^* \leq 0.08$), relative roughness (0.08

Author-produced version of the article published in Earth Surface Processes and Landforms , 2018
The original publication is available at https://onlinelibrary.wiley.com/doi/abs/10.1002/esp.4322
doi : 10.1002/esp.4322

$\leq D/h \leq 0.14$) and bed morphology planform (plane or braided beds) (Camenen et al., 2010).

Bed material

Two types of bed materials were studied: moderately sorted gravel (G) and bimodal material composed of the same gravel matrix infiltrated with fine sediments (Figure 2). Three types of fine sediment were used: two were non-cohesive (sand (S) and artificial fine sand (FS)) and one was cohesive (medium silt (Ms)). Table 1 summarizes the geometrical and geotechnical characteristics of gravel and fine sediments. Hereafter, D and d denote diameters of the coarse (G) and fine (S, FS or Ms) sediments, respectively.

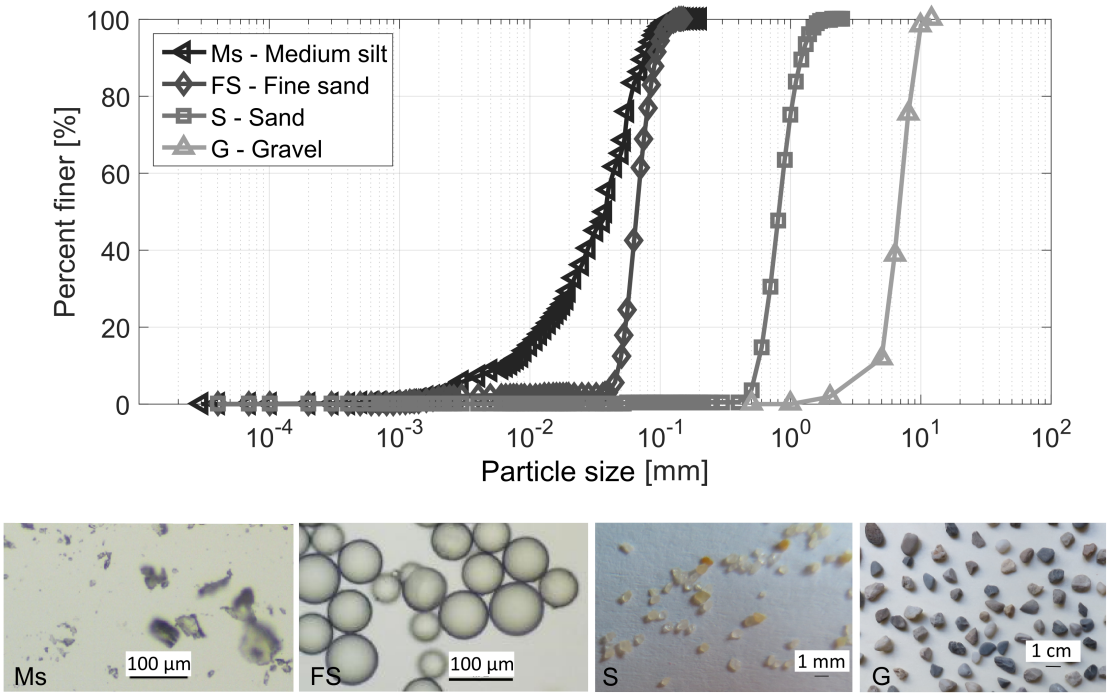

Figure 2: Sediment GSD and shapes. Photographs of Ms and FS were taken with a microscope.

Gravel was quite angular with $D_{50} = 6.8\,\mathrm{mm}$, where D_i is the diameter such that i % of grains are finer by weight. Sand was natural and well sorted, with a median diameter $d_{50} = 813\,\mu\mathrm{m}$. Fine Sand (FS) consisted of non-cohesive glass

beads with $d_{50} = 66\,\mu$m. Medium silt (Ms) was formed of cohesive glass powder, with $d_{50} = 40\,\mu$m, whose size is similar to FS.

The circularity index C_I was chosen as the shape indicator (Table 1). It measures the 2D grain shape deviation from a perfect circle (changes in grain form, symmetry or roughness). C_I was computed using image-post-processing of each sediment shape (Figure 2, $C_I = 4\pi A/P^2$, with A as the area of the particle projected on the image and P the perimeter of the projected area). Around 50 particles of each sediment material were analysed to obtain statistically relevant indexes. $C_I = 1$ is associated with a perfect circle, whereas $C_I \approx 0$ indicates a distorted shape.

Consolidation of fine sediments, C_u, was determined using a penetrometer (French norms, XP CEN ISO/TS 17892-6, 2006) and a scissometer (French norms, NF P 94-072, 1995). In the penetrometer test, C_u corresponds to a dynamic penetration resistance, whereas in the scissometer test, C_u is the sediment resistance to a rotational moment. C_u reported in Table 1 are averaged values given by these two tests. Tests were performed on water-saturated ($C_{u\text{-sat}}$) and low water content ($C_{u\text{-20-30\%}}$) sediment samples. For Ms, C_u reaches values similar to those characterizing soft rocks ($\geq 250\,$kPa) when the water content is low.

Figure 3 illustrates the gravel beds tested. Beds are identified and named according to the following nomenclature: *bed arrangement of the gravel matrix* (L for loose, H for hybrid and P for packed) and *sediments forming the bed material* (G for gravel, S for sand, FS for fine sand and Ms for medium silt). The following sections describe how these beds were prepared.

Experimental procedure for clean gravel beds

Preparation of clean gravel beds - Both loose and packed (L-G and L-P) clean gravel beds were studied. L-G beds denote loose, random and non-organized gravel beds that were not subjected to antecedent flows. To create L-G beds, gravel was manually installed in the flume using a large scraper to obtain an 8 cm-thick flat bed surface, parallel to the flume bottom. In contrast, antecedent long flows over a

Author-produced version of the article published in Earth Surface Processes and Landforms , 2018
The original publication is available at https://onlinelibrary.wiley.com/doi/abs/10.1002/esp.4322
doi : 10.1002/esp.4322

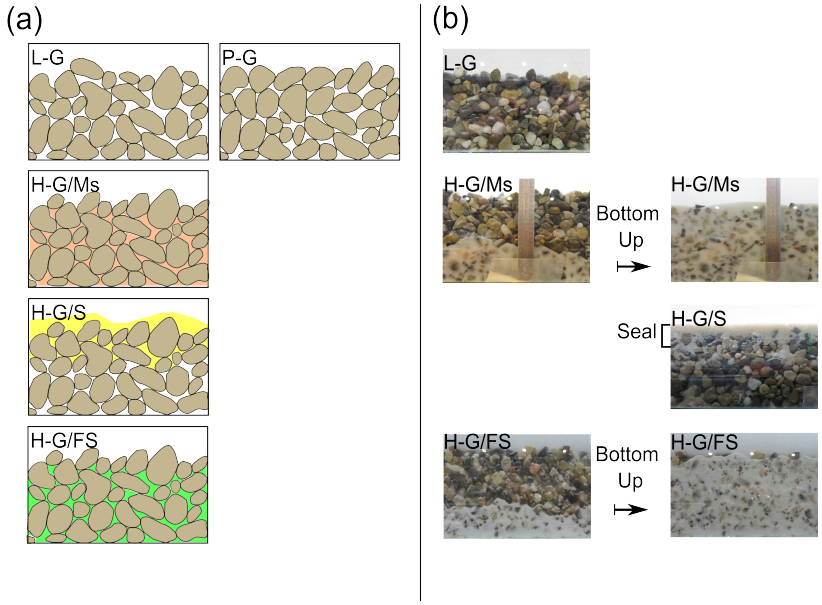

Figure 3: (a) Diagrams illustrating the beds studied and (b) lateral photographs of the beds during (left) and at the end (right) of the infiltration phase.

gravel bed were necessary to create a packed and structured bed (P-G bed). The P-G bed preparation followed three steps (Figure 4a). In step (1), a L-G bed was prepared. In step (2), this bed was subjected to a typical flood hydrograph with increasing and decreasing steps of 5 L/s. At the end of step (2), a hybrid bed (H-G) was obtained, defined as a bed that had just experienced a flood for a short time. The flow discharge $Q_{\text{ref-F}}$ producing a specified reference transport rate $q_{s\text{-ref}}$ at the falling limb in step (2) was determined. $q_{s\text{-ref}}$ refers to the first low bedload rate, that can be accurately measured considering the large uncertainty linked to bedload measurement at low bed shear stresses. $q_{s\text{-ref}}$ defines the gravel incipient motion and should be adapted if a different gravel material was studied (USWES, 1935; Parker et al., 1982). In this case, $Q_{\text{ref-F}}$ corresponds to the discharge for cessation of gravel motion on a hybrid bed (i.e. for which gravel transport becomes lower than $q_{s\text{-ref}}$). This discharge was not exactly the same between two experiments because we were not able to reproduce the exact same initial loose bed ($Q_{\text{ref-F}}$ was within the range of 60 - 65 L.s^{-1}). The difficulty to reproduce loose beds was highlighted by analysing the laser scanner surveys of their bed surfaces. Laser scanner data also show that grain arrangements were present on a H-G bed, although not as

Author-produced version of the article published in Earth Surface Processes and Landforms , 2018
The original publication is available at https://onlinelibrary.wiley.com/doi/abs/10.1002/esp.4322
doi : 10.1002/esp.4322

pronounced as for a P-G bed. Step (3a) is the arrangement phase. A constant discharge of $Q_{\text{ref-F}}$ was imposed for several hours to enhance a natural bed surface arrangement. This arrangement phase was stopped when the gravel transport rate became insignificant at the downstream end of the flume, i.e., after approximately 12 hours. We considered that the P-G bed is created at the end of step (3a). Water was then drained out carefully from the flume, keeping the P-G bed surface organization intact. Since the P-G bed preparation was carried out with low gravel transport, the bed stabilized without significantly changing its longitudinal slope (variation was around 5 % on average).

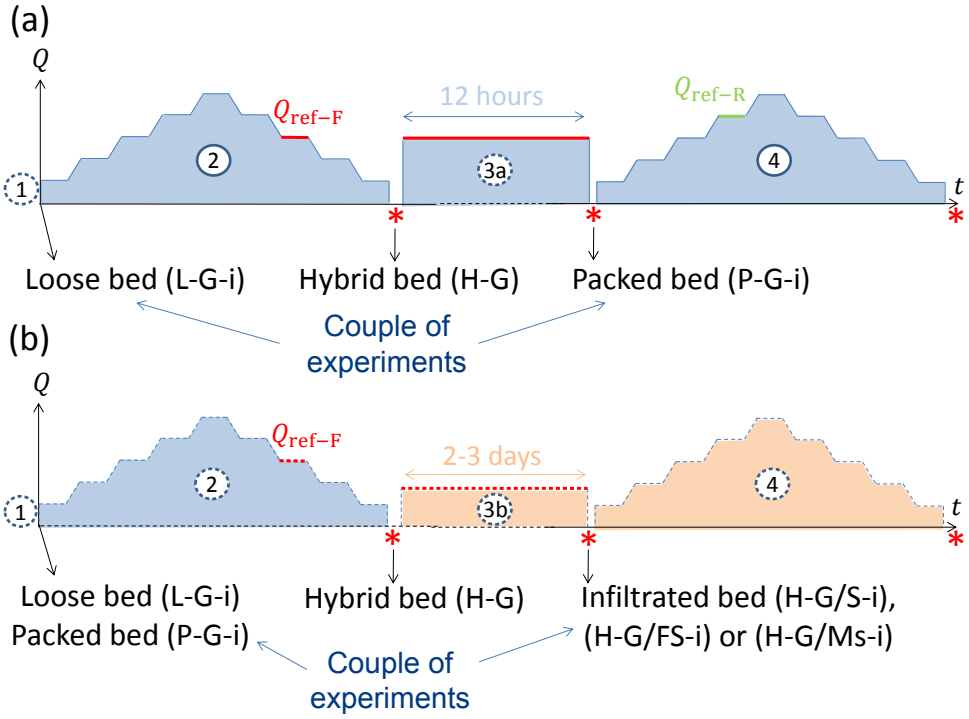

Figure 4: Experimental protocol from bed preparation to bedload experiment for a) clean gravel beds and b) infiltrated gravel beds. Blue areas correspond to clear water flow while orange areas represent fine concentrated water flow. (1) denotes the bed installation, (2) and (4) refer to sediment transport experiments. (3a) and (3b) are bed arrangement phase and infiltration phase, respectively. The symbol * indicates a drained bed (which can last a few days). $Q_{\text{ref-R}}$ and $Q_{\text{ref-F}}$ are the flow discharges for which the initiation of gravel motion (during the rising limb) and the cessation of gravel motion (during the falling limb) were observed, respectively.

Sediment transport experiments on clean gravel beds - For the sake of clarity, each test is denoted with the bed nomenclature completed by a number i. Two experiments sharing the same number refer to one *experiment couple*,

corresponding to two tests performed successively with no manual gravel bed re-installation (steps (2) and (4) in Figure 4). For example, a loose bed experiment conducted before a bed arrangement phase forms a couple with the next packed bed experiment (e.g. L-G-1 followed by P-G-1). Similarly, two experiments conducted before and after the infiltration phase form a couple (e.g. L-G-5 and H-G/Ms-5).

A sediment transport experiment consisted in operating the flume with a stepped flow hydrograph while collecting transported gravel periodically at the flume's downstream end (Figure 4, step (2) for L-G and step (4) for P-G). The selected hydrographs simulate unsteady flow events, characterized by symmetrical rising and falling limbs with steady and uniform flow intervals lasting 15 - 20 min and flow transitions lasting 5 min. Stepped plateaus provide steady flows that can more easily be characterized than a true unsteady flow. In addition, the characteristic time for bed arrangement was found to be much longer (several hours) (Church et al., 1998) than the plateau duration. Consequently, we expected the flow to be unsteady from the sediment transport point of view. Similar hydrographs (i.e., magnitude, duration and sequencing) were used for all experiments so that they could be compared (see supplementary files). Before starting each experiment, the bed surface was photographed and scanned. The transported gravel was collected every 5 min (three times per interval) in the rolling sieves at the downstream end of the flume and was then dried and weighed to deduce bedload temporal variations (per unit width) $q_s(t)$. Using recorded videos, $q_s(t)$ was estimated by visually counting gravel passing through a given area at different locations (i.e., upstream, middle, and downstream of the channel). The measured bedload rate at the downstream end of the flume was roughly the same as the one estimated from visual counting; the observed differences may be the consequence of local variation and long bedload oscillation since q_s is averaged over several minutes (Recking et al., 2012). The level of the water surface was measured during each hydrograph plateau at every meter along the flume centerline; the averaged water depth h was then calculated. After each sediment transport experiment, the bed was drained and a topographic survey was carried

out.

Experimental procedure for infiltrated beds

Preparation of infiltrated beds - Bimodal beds (H-G/Ms, H-G/FS, H-G/S) were not prepared by homogeneously mixing gravel and fine sediments as commonly done in previous studies (Wilcock et al., 2001; Curran and Wilcock, 2005). Instead, bimodal beds were prepared by infiltrating fines into a H-G bed, thereby replicating natural vertical bed structures (Figure 3). Figure 3b shows a side view of the final beds at the end of each infiltration operation. Table 1 summarizes the geotechnical properties of the bed materials tested except for the case of a bed infiltrated with sand particles. Indeed, no average values were estimated for this case because of the inhomogeneous vertical distribution of sand through the gravel matrix.

Figure 4b illustrates how a bimodal bed was prepared. First, a sediment transport experiment (step (2)) was carried out on a specific initial bed (i.e., L-G or P-G) to obtain a hybrid bed. The bed is designated as hybrid when produced using a single hydrograph flowing either over a L-G bed or over a P-G bed. In the bimodal experiments, only experiment H-G/Ms-6 resulted from an initial P-G bed. Hybrid beds are more reproducible in the laboratory in terms of bed surface arrangements than loose beds, which is why the infiltration phase (step (3b)) was performed on such beds. An infiltrated hybrid bed and a clean hybrid bed can be compared by focusing only on the effect of fine sediment presence and by excluding the potential effects of changes in bed arrangement.

For the preparation of H-G/FS and H-G/Ms beds, a fine sediment-laden flow recirculated along the flume under flow conditions yielding no gravel motion. For these beds, the D_{15}/d_{85} ratio, representing the capacity of the coarsest fine grains (d_{85}) to get through the finest coarse grains (D_{15}), was larger than 150. According to Gibson et al. (2009), USP is the expected infiltration mechanism for $D_{15}/d_{85} \geq 15.4$, meaning that fine sediments should fill the beds from the bottom upwards. This was indeed verified (see the evolution of the infiltration in Figure 3b, lines 2

and 4). To keep an approximately constant concentration during the infiltration phase (step (3b)), bags of fine sediments were added periodically to the water tank. The infiltration phase stopped when the bed was fully clogged, i.e., when gravel matrix pores were fully filled by fines. The flow discharge was then cut off and the bed was carefully drained.

A similar protocol was used to prepare a H-G/S bed, except during the infiltration phase (step (3b)). The sand was too coarse to recirculate mixed with the water. Therefore, a feeding system located at the flume entrance supplied sand continuously and uniformly across the channel width. During step (3b), sand moved as bedload along the flume. Sand particles entered the gravel matrix but were quickly trapped within the gravel pore spaces near the bed surface, thereby blocking infiltration deeper into the substrate and creating a bridge (or seal). This behavior is consistent with the findings reported by Gibson et al. (2009) who stated that bridging should occur for $D_{15}/d_{85} \leq 10.6$ (for the present H-G/S bed, D_{15}/d_{85} was equal to 4.5). Step (3b) was stopped when a sand bridge at the surface was stable along the entire flume length. Flow and sand feedings were cut off and the bed was carefully drained.

Sediment transport experiment on infiltrated beds - For the H-G/FS experiment, the stepped hydrograph and the bedload sampling time were similar to those used for the clean gravel bed experiments (L-G and P-G). For the other infiltrated beds, the protocol for the sediment transport experiments was slightly different. For the H-G/Ms experiments, the maximum flow magnitude was increased because the presence of Ms particles reduced the gravel rate. For the H-G/S experiment, the steady flow plateaus were reduced in time (8 min instead of 15 or 20 min) and magnitude (see supplementary files) because sand increased the gravel transport. Reducing the duration of each flow plateau prevented significant bed changes. Bedload was measured at the downstream end of the flume every 4 min. During this experiment, sand was fed at the same rate as the infiltration phase. For the H-G/FS and H-G/Ms experiments, fines recirculated at the same concentration as the end

Author-produced version of the article published in Earth Surface Processes and Landforms , 2018
The original publication is available at https://onlinelibrary.wiley.com/doi/abs/10.1002/esp.4322
doi : 10.1002/esp.4322

of the infiltration phase.

Results

Bedload rate over clean gravel beds

Figure 5 shows the temporal variation of flow and bedload rates for the L-G-7 test, which is representative of all tests carried out with L-G and P-G beds (see supplementary files); the results differ only in terms of bedload intensity, which depends on the initial surface bed arrangement. The bedload rate q_s increases and decreases with flow discharge, following a single-peak shape. At each of the hydrograph plateaus, the first of the three measured bedload rates is often the highest one (Figure 5), particularly during the rising limb period. This may reflect the temporal variability and the beginning of the decline observed in many studies at a constant flow discharge (Hassan et al., 2006; Recking et al., 2012; Guney et al., 2013).

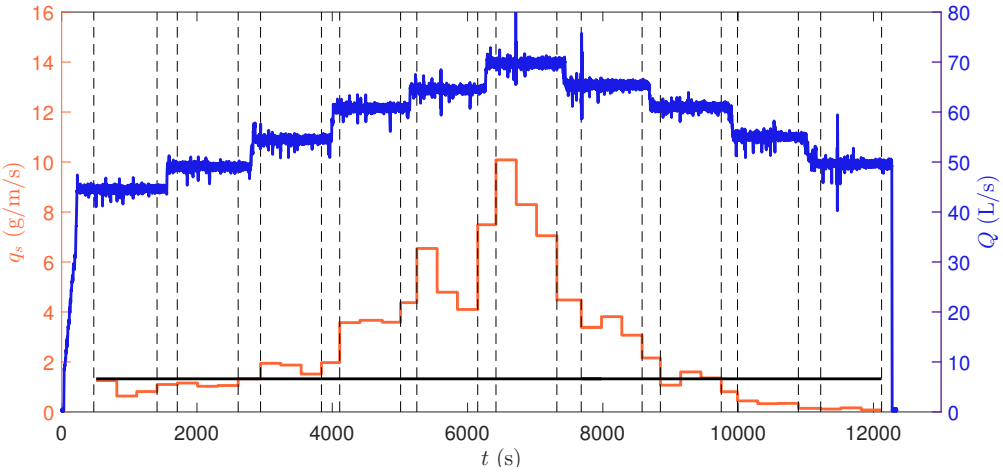

Figure 5: Time variations of bedload rates (in orange) and flow (in blue); results for L-G-7 test. Grid delimits steady states from transition zones. Black horizontal line corresponds to the reference transport rate $q_{s\text{-ref}} = 1.325\,\mathrm{g.m^{-1}.s^{-1}}$.

The evolution of the dimensionless bedload rate $q_s^* = q_s/\sqrt{(s-1)gD_{50}^3}$ as a function of the dimensionless bed shear stress $\tau^* = \tau/\left[(\rho_s - \rho)gD_{50}\right]$ (where $\tau = \rho g R_h J$ is the bed shear stress, $s = \rho_s/\rho$ is the relative grain density, ρ and ρ_s are the

Author-produced version of the article published in Earth Surface Processes and Landforms , 2018
The original publication is available at https://onlinelibrary.wiley.com/doi/abs/10.1002/esp.4322
doi : 10.1002/esp.4322

water and sediment density, respectively, g is the gravitational acceleration, R_h is the hydraulic radius corrected for side-wall effects following the method of Vanoni and Brooks (1957), J is the energy slope set at the bed slope for uniform flow and D_{50} is the representative median diameter of gravel particles present on the bed surface) is examined in Figure 6. $D_{50} = 6.8$ mm was assumed for all the calculations, even for packed beds, because significant surface grain coarsening was not observed.

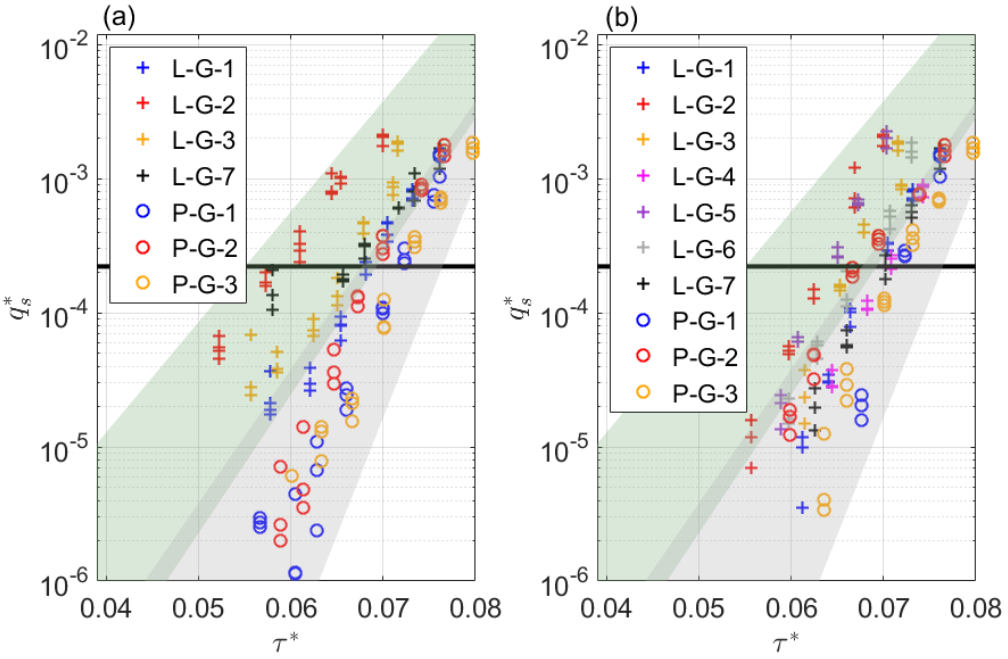

Figure 6: Evolution of the dimensionless bedload rate with dimensionless bed shear stress; results for the clean L-G and P-G beds: (a) at the rising limb and (b) at the falling limb. Green and grey shaded areas delimit loose bed data and packed bed data, respectively, during the rising limb. These areas are reported on Figure 6b. Black horizontal line corresponds to $q^*_{s\text{-ref}} = 2.2{\times}10^{-4}$.

For the sake of clarity, the bedload rates during flow transitions are not shown in Figure 6. The results related to rising and falling limbs are separated to capture any possible differences in bedload evolution. Three or four q_s^*-values are available for a given τ^*-value (i.e., given flow discharge). At very low bed shear stresses, the bedload fluctuated substantially, making high-accuracy measurements delicate (Ancey et al., 2015). The inter-comparison of tests at very low bed shear stress is therefore not appropriate. The dimensionless reference transport rate $q^*_{s\text{-ref}}$ associated with the reference transport rate $q_{s\text{-ref}} = 1.325\,\mathrm{g.m^{-1}.s^{-1}}$, defined in the protocol as the

gravel's incipient motion, is shown. $q^*_{s\text{-ref}} = 2.2{\times}10^{-4}$ corresponds to the lowest, sufficiently accurate, measured dimensionless bedload rate. Above this reference rate, the scatter of q^*_s is reduced and comparisons between the diverse experiments are possible (Figure 6). It should be noted that $q_{s\text{-ref}} = 1.325\,\mathrm{g.m^{-1}.s^{-1}}$ is larger than the reference rate calculated from the dimensionless parameter ($W^* = q^*/\tau^{*3/2}$) proposed by Parker et al. (1982). According to these authors, the incipient motion for gravel particles is attained for $W^* = 0.002$, namely with q_s around $0.2\,\mathrm{g.m^{-1}.s^{-1}}$ in the present experiments. This rate is too low and ought to be subjected to large measurement uncertainty. Retaining $q_{s\text{-ref}} = 1.325\,\mathrm{g.m^{-1}.s^{-1}}$ leads to $W^* = 0.01$ in the present tests.

Figure 6 shows that loose and packed beds behave differently. For a given q^*_s-value, τ^* is globally lower for loose beds than for packed beds, particularly during the rising limb. Comparing one *experiment couple* during the rising limb, the reference dimensionless bed shear stress τ^*_{ref} (i.e., the dimensionless bed shear stress needed for generating the bedload rate $q^*_{s\text{-ref}}$) for the packed bed can be from 5 % to 19 % higher than for the loose bed (on average 12 %). We expected that all the data would collapse for one type of bed (either L-G or P-G) since the same protocol was applied. However, there are significant differences between two L-G experiments (see L-G-1 and L-G-2, for example) and they cannot all be explained by the measurement uncertainty. We believe that the initial bed arrangement is the main cause for these differences. Nevertheless, two main areas encompass all data related to L-G experiments (green shaded area) and data related to P-G experiments (grey shaded area), respectively (see Figure 6a). The scatter due to the temporal variability of bedload (several q^*_s-values for one given τ^*-value) does not question these two distinct areas. The intersection of these areas provides a location for data related to tests on a slightly packed bed. During the falling limbs (Figure 6b), there are fewer differences between loose and packed beds than during the rising limb. The reference dimensionless bed shear stress τ^*_{ref} decreases for P-G beds and increases for L-G beds. The data tend to gather in a single area: the intersection area mentioned

Author-produced version of the article published in Earth Surface Processes and Landforms , 2018
The original publication is available at https://onlinelibrary.wiley.com/doi/abs/10.1002/esp.4322
doi : 10.1002/esp.4322

above. This behavior characterizes hybrid beds. Somehow, the hydrograph seems to reset previous shear stress histories, so that both hybrid beds resulting from a loose or a packed bed present similar bedload dynamics and similar bed surface arrangements.

Bedload hysteresis patterns are observed for both bed configurations (Figure 6). Clockwise hysteresis (i.e., bedload rates that are larger during the rising limb than during the falling limb for the same shear stress) are observed for L-G beds, but either no hysteresis or counter-clockwise hysteresis are noted for P-G beds. These results reveal a close connection between bedload rate and gravel bed arrangement. Figure 7 illustrates the hysteresis patterns for the experiment couple n°2, namely a clockwise loop for L-G-2 and a counter-clockwise loop for P-G-2. For L-G beds, gravel particles are easily transported during the rising limb while re-arranging and strengthening the bed. Consequently, bedload rates become lower during the falling limb. For P-G beds, the opposite behavior is observed. The bed is initially packed and the gravel transport is initiated for higher bed shear stresses. During the rising limb, grain structures can be broken and the bed surface can become weak if the bed shear stress reaches sufficient values. In that case, the mobility of gravel is enhanced during the falling limb. Otherwise, bedload remains approximately the same during the falling and rising limbs.

Bedload rate over infiltrated beds

Figure 8 presents data related to infiltrated bed experiments and shows the evolution of q_s^* with the dimensionless shear stress τ^*. Previous areas defined for clean gravel beds (Figure 6) are recalled in Figure 8 for comparison.

During the rising limb, bedload rates for the H-G/FS bed are similar to those observed during the falling limb for L-G beds (close to the intersection area), indicating that FS has no influence on gravel dynamics. However, during the falling limb, the H-G/FS bed behaves differently. Data remain in the same area as during the rising limb, but τ^*_{ref} is smaller. The evolution of bedload follows a counter-clockwise

Author-produced version of the article published in Earth Surface Processes and Landforms , 2018
The original publication is available at https://onlinelibrary.wiley.com/doi/abs/10.1002/esp.4322
doi : 10.1002/esp.4322

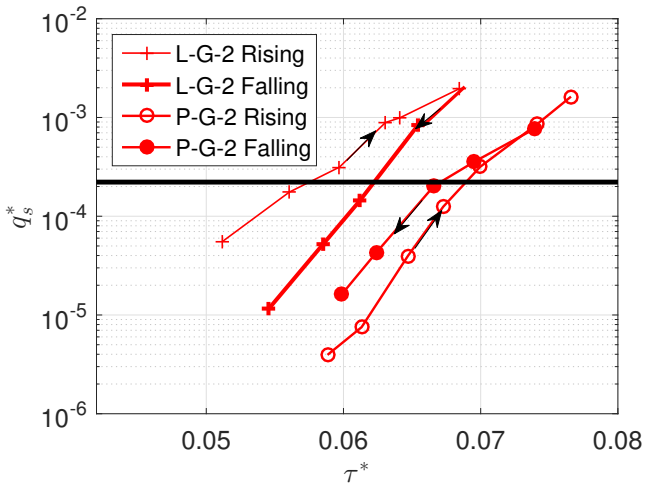

Figure 7: Bedload hysteresis patterns for L-G-2 and P-G-2. Black arrows indicate the hysteresis direction. Black horizontal line corresponds to $q^*_{s\text{-ref}} = 2.2\times10^{-4}$. The bedload rates presented here correspond to values averaged over each steady plateau.

loop, which was not the case for L-G experiments. The gravel transport during the falling limb was thus enhanced compared to the rising limb: FS was rapidly washed from the bed surface and progressively from the substrate. At the falling limb, FS reached a sufficient concentration within the water column to result in a gravel-fine interaction. FS sediments affect bedload during the falling limb by lubricating the bed.

Results for the H-G/Ms beds gather in the area that previously corresponds to P-G bed data during the rising limb (Figure 8a). In our case, clogging with cohesive Ms has similar effects on bed mobility as gravel arrangement. In addition, data from H-G/Ms-6 have the same behaviour than the other data from H-G/Ms experiments, even if the bed resulted from an initial P-G bed. The lack of difference within hybrid beds is once again verified. Data from H-G/Ms tests follows counter-clockwise hysteresis, meaning that the transport of gravel is enhanced during the falling limb, except in the H-G/Ms-5 test that shows a clockwise hysteresis. This exception will be discussed in the Discussion Section. During the rising limb, Ms is more difficult to wash out of the bed surface than FS because of its cohesion. Gravel mobility is reduced due to the presence of cohesive Ms. During the falling limb, the infiltrated gravel bed is partially cleaned from Ms, and then tends to behave like a

Author-produced version of the article published in Earth Surface Processes and Landforms , 2018
The original publication is available at https://onlinelibrary.wiley.com/doi/abs/10.1002/esp.4322
doi : 10.1002/esp.4322

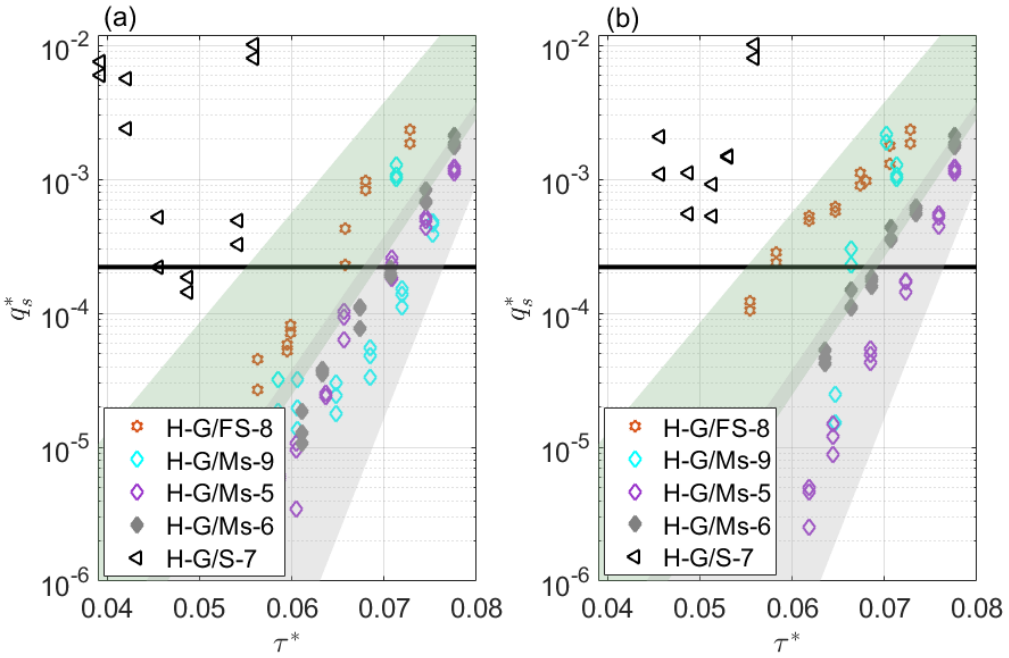

Figure 8: Evolution of the dimensionless bedload rate with dimensionless bed shear stress; results for infiltrated gravel beds: (a) at the rising limb and (b) at the falling limb. Green and grey shaded areas are the same as presented in Figure 6. The open and closed symbols denote data obtained on hybrid beds resulting from initial loose and packed beds, respectively. Black horizontal line corresponds to $q^*_{s\text{-ref}} = 2.2\times10^{-4}$.

clean H-G bed.

For the gravel bed infiltrated with sand (H-G/S-7), the highly scattered bedload rates make the results difficult to interpret. Figure 8 shows a new area for the H-G/S experiment, with high bedload rates for τ^*-values being much lower than those for the other experiments. The seal of sand clearly enhanced the gravel transport. No hysteresis loop is identifiable and no single τ^*_{ref} could be defined during the rising and falling limbs. Figure 9 shows the evolution of bedload as a function of time and hydraulic conditions, to be compared to Figure 5 (L-G-7 test). Contrary to L-G-7, bedload evolution in H-G/S-7 shows a two-peak shape (Figure 9). The first bedload peak observed at very low flow discharges is probably caused by the presence of the bridge of sand lubricating the bed surface. The second peak appears at a flow discharge of around 60 L/s, similar to the increase in bedload for L-G-7 (Figure 5). However, the bedload rate is six times higher when sand is present.

Author-produced version of the article published in Earth Surface Processes and Landforms , 2018
The original publication is available at https://onlinelibrary.wiley.com/doi/abs/10.1002/esp.4322
doi : 10.1002/esp.4322

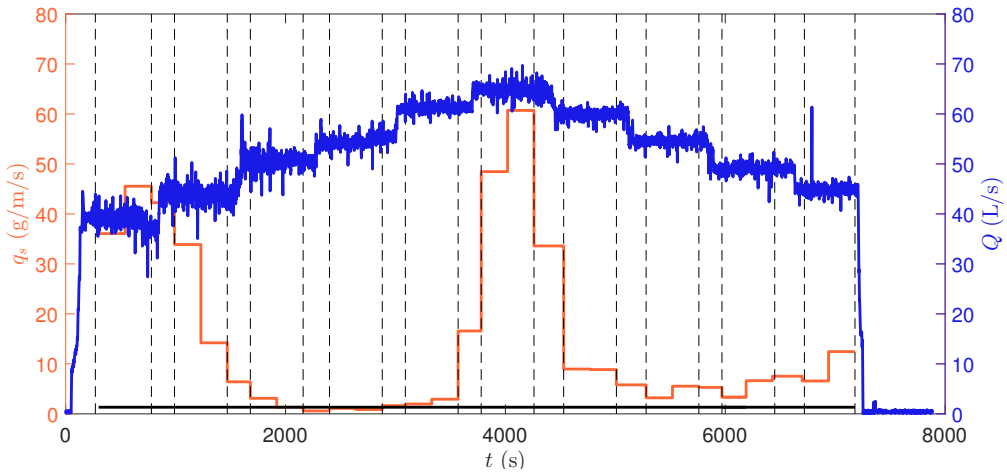

Figure 9: Time variations of bedload rates (in orange) and flow (in blue); results for the H-G/S-7 test. Grid delimits steady states from transition zones. Black horizontal line corresponds to $q_{s\text{-ref}} = 1.325\,\mathrm{g.m^{-1}.s^{-1}}$.

Summary of the results

Figure 10 shows a schematic temporal evolution of different beds responding to similar bed shear stresses. This Figure highlights significant steps generating substantial changes in the bed matrix composition and in sediment transport ($T0$ - $T5$). In one line, the absence of a box means that no significant change occurred between the time considered and the previous time. Values of τ^*_{ref} are represented with horizontal bold color lines and plotted on the evolution graph (τ^*, t) for each type of bed. Each color is associated with one specific bed (see colors of the box edges). $\tau^*_{\text{ref-R}}$ corresponds to the dimensionless bed shear stress for which the initiation of motion during the rising limb was observed and $\tau^*_{\text{ref-F}}$ corresponds to the dimensionless bed shear stress for which the cessation of sediment motion was observed during the falling limb. The bed arrangement and degree of clogging described at $T5$ refer to the final bed state (T_f).

Loose and packed beds (L-G and P-G) - A loose bed is put into motion ($T2$) before a packed bed ($T3$) (red and black boxes in Figure 10). For the L-G bed, q_s is higher than the reference value $q_{s\text{-ref}}$ between $T2$ and $T5$. During this time lapse, the L-G bed packs and organizes itself. The resulting bedload rate during the falling limb is lower than during the rising limb for the same bed shear

Author-produced version of the article published in Earth Surface Processes and Landforms , 2018
The original publication is available at https://onlinelibrary.wiley.com/doi/abs/10.1002/esp.4322
doi : 10.1002/esp.4322

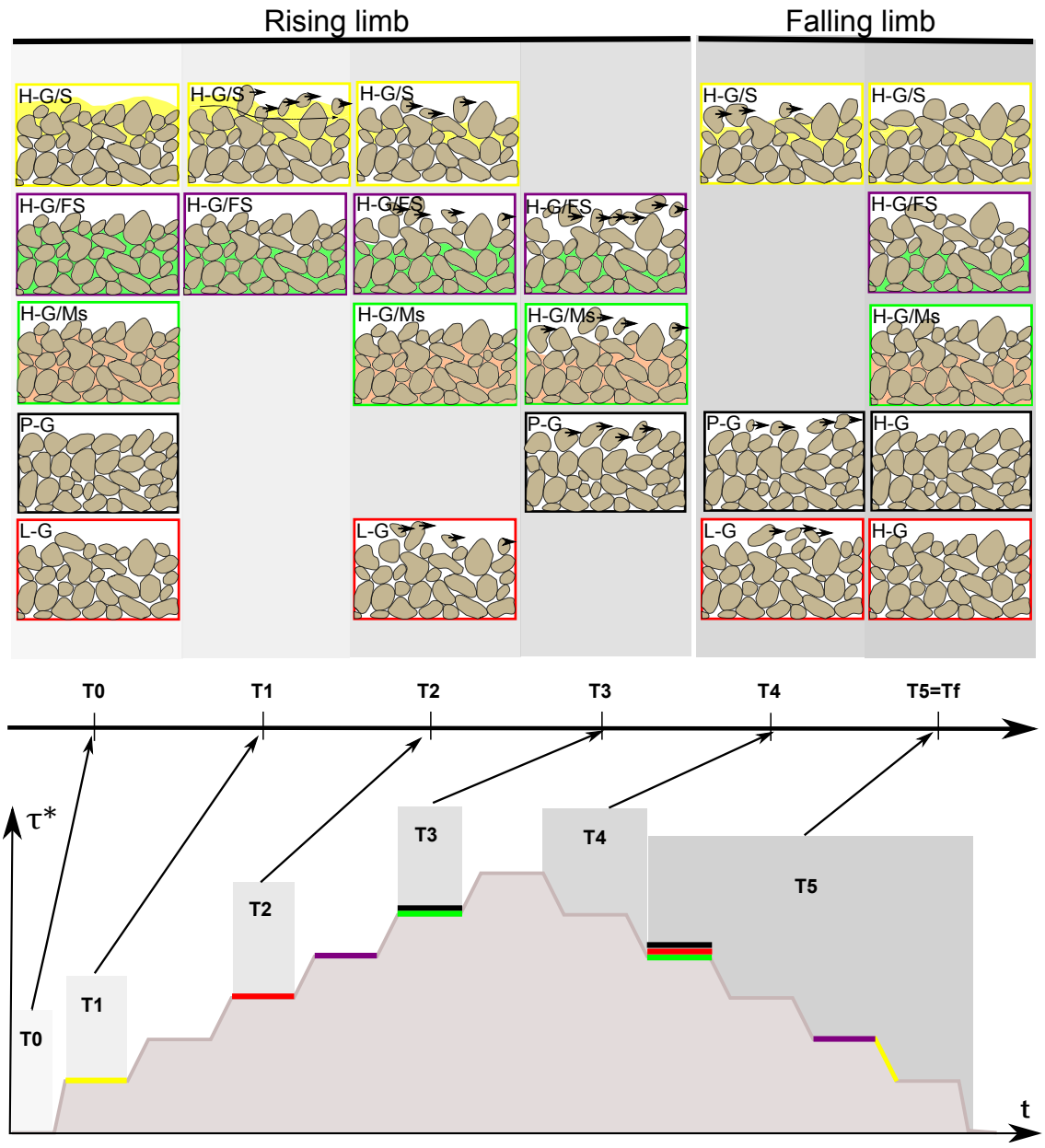

Figure 10: Description of the different bed evolutions during a hydrograph. Each line in the upper part describes how a specific bed evolves during the hydrograph schematized below. A color is attributed to each bed type (contour of the box). Key times in this evolution are denoted $T0$ to $T5$ and represented by shaded columns on both hydrograph and upper part of the diagram. A missing box in the line means that no change occurred between the time considered and the previous time. Horizontal color lines on the hydrograph correspond to $\tau^*_{\text{ref-R}}$ and $\tau^*_{\text{ref-F}}$ for each bed type. Arrows inside the boxes represent gravel transport. They are not scaled according to the sediment transport intensity.

Author-produced version of the article published in Earth Surface Processes and Landforms , 2018
The original publication is available at https://onlinelibrary.wiley.com/doi/abs/10.1002/esp.4322
doi : 10.1002/esp.4322

stress (clockwise hysteresis). The opposite is observed for the packed bed (counter-clockwise hysteresis), meaning that the flow has probably started to break grain arrangements initially present on the bed surface ($T3$ - $T4$). The final states of both beds tend to become similar as well as the reference dimensionless bed shear stress $\tau^*_{\text{ref-F}}$. A hybrid bed H-G is obtained.

Beds infiltrated with Ms (H-G/Ms) - The following description of the H-G/Ms behaviour is suitable for both hybrid beds resulting from an initial loose bed or packed bed. At the beginning of the rising limb ($T0$ - $T1$), gravel particles forming the H-G/Ms bed (green boxes) are totally enclosed by fine consolidated sediments. The bed surface layer of the matrix is first washed of its fine sediments ($T2$). At $T3$, gravel is transported at the same $\tau^*_{\text{ref-R}}$ as the P-G bed while fine sediments are still washed from the bed. In our experiments, cementation and packed arrangement have effects of similar magnitude on gravel transport. During the falling limb, the bed behaves in the same way as a H-G bed. At $T5$, the H-G/Ms bed surface tends to become similar to the H-G bed surface, as well as the associated $\tau^*_{\text{ref-F}}$.

Beds infiltrated with FS (H-G/FS) - During the rising limb, a H-G/FS bed (purple boxes) evolves similarly to a H-G bed, because fines are easily and quasi-instantaneously ($T1$) washed out of the bed surface. As the τ^* peak is reached, FS is preferentially put into suspension, causing an increase in fine sediment concentration into the flow ($T3$). It is important to recall that FS was recirculated with water. This high concentration lubricates the bed surface, enhancing the gravel transport ($T3$ - $T4$). The shape of FS is spherical (Figure 2), which may favor this lubrication. During the falling limb, no strong organization is observed. The significant gravel transport prevents particle organizations. If conditions of low bedload were longer, grain organizations might appear. At Tf, the bed surface is significantly loose with $\tau^*_{\text{ref-F}}$ lower than in the other cases described above.

Beds infiltrated with S (H-G/S) - As shown in Figure 9, the bedload evolution for the H-G/S bed (yellow boxes) is marked by two main stages. First, at low-flow discharge during the rising limb ($T1$), the bed surface is highly concentrated

Author-produced version of the article published in Earth Surface Processes and Landforms , 2018
The original publication is available at https://onlinelibrary.wiley.com/doi/abs/10.1002/esp.4322
doi : 10.1002/esp.4322

in sand, which lubricates and facilitates gravel particles rolling around their neighbours. The equal mobility phenomenon was observed, meaning that gravel particles are transported as easily as sand (Parker et al., 1982). The highly concentrated sand layer starts moving as bedload on the bed surface. The moving sand particles collide with gravel particles, destabilize them and finally entrain them. As the sand layer is washed from the bed surface, gravel transport decreases. Although there was sand feeding during this experiment, it was not sufficient to maintain a high concentration at the surface layer; consequently the gravel transport rate decreased. Once τ^* reaches the reference value $\tau^*_{\text{ref-R}}$ found for the L-G tests, significant gravel transport is observed again ($T2$). Even if the sand concentration infiltrated into the bed is relatively low compared to what was on the bed surface at the beginning of the experiment, it is still high enough to enhance the transport of gravel ($T3$ - $T5$). The intensity of this effect may be attributed to the fact that sand and gravel are mainly transported as bedload.

Discussion

Impact of bed arrangement

Under similar hydraulic conditions (see supplementary files), diverse bedload rates were observed for beds composed with the same material (same GSD) having different levels of arrangements. The arrangements of L-G and P-G beds were quantified using the laser scanner. The analysis of the three-dimensional topographic surveys of the bed surfaces revealed substantial changes between the two types of bed (Marion et al., 2003; Mao et al., 2011; Perret et al., 2016).

The geometrical grain roughness of the bed surface (σ_{zg}) was found to be smaller for P-G beds than for L-G beds, revealing a better bed surface particle imbrication and thus a smoother bed surface for packed beds. Small bedforms (preferential pathways) and bed structures were present on P-G bed surfaces. Structure lengths in the streamwise (Δ_{x0}) and the cross-stream direction (Δ_{y0}) were about $2\times D_{50}$.

Gravel particles were orientated in the streamwise direction for P-G beds, whereas they were randomly organized in L-G beds (Nikora et al., 1998; Marion et al., 2003). The drag force for gravel orientated in the streamwise direction is on average smaller than for randomly orientated gravel. In addition, a decrease in bed surface roughness should lead to lower flow resistance as well (Smart et al., 2002). Gravel transport should therefore be reduced for the P-G experiments in comparison to the L-G tests considering the same hydraulic conditions. This is consistent with our results (see Figure 6). Topographic surveys made at the end of each sediment transport experiments were also analyzed and showed that bed surfaces were quite similar for hybrid beds (resulting from a loose or a packed bed) in terms of bed roughness, imbrication and grain orientation.

We have seen that results from loose and packed beds at the falling limb (i.e. hybrid beds, see Figure 6) form a scattered data set among which both beds can not be distinguished. The lengths of the bed forms at the end of the experiments show also a significant scatter. This scatter is nevertheless lower for the grain roughness, which is the source of skin friction. It should be recalled that the total bed shear stress τ can be broken down into a bed shear stress component due to grain resistance, τ_g, and a bed shear stress component due to form resistance, τ_f. Sediment motion is generally attributed to the skin friction τ_g and not to the total shear stress τ (Petit et al., 2015). To further investigate the part of bed forms in the scatter of our data and focus on grain scale, we estimate the skin friction to analyse sediment transport rate in our experiments.

Figure 11 shows q_s^* as a function of τ_g^*, computed using the Manning-Strickler equation and a Strickler coefficient $K_g = 21/D_{50}^{1/6}$, which represents skin roughness assumed to be identical for all experiments conducted on clean beds:

$$\tau_g = \rho g \left(\frac{Q}{W\sqrt{J}K_g} \right)^{3/5} J \tag{1}$$

where W is the channel width.

The same trend as in Figure 6 is replicated in Figure 11, namely two dimension-

Author-produced version of the article published in Earth Surface Processes and Landforms , 2018
The original publication is available at https://onlinelibrary.wiley.com/doi/abs/10.1002/esp.4322
doi : 10.1002/esp.4322

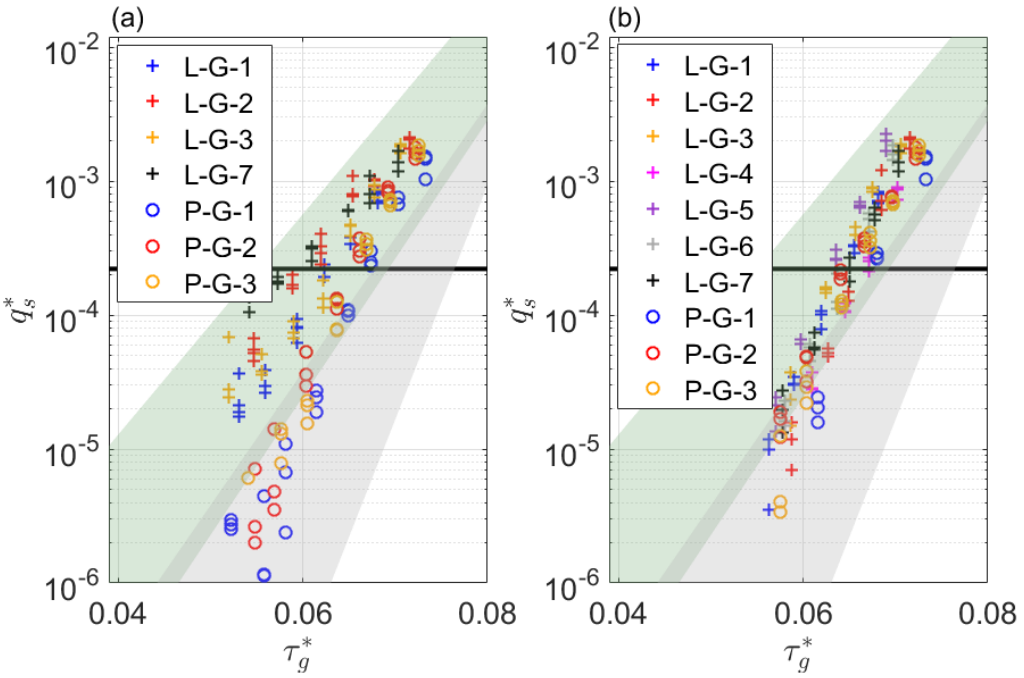

Figure 11: Evolution of the dimensionless bedload rate with dimensionless skin friction: (a) rising and (b) falling limbs data. Gray and green shaded areas are the same as in Figure 6. Black horizontal line corresponds to $q^*_{s\text{-ref}} = 2.2{\times}10^{-4}$.

less bed shear stress zones are present during the rising limb versus one area during the falling limb. Assuming the same bed roughness for all the clean beds during the falling limb seems reasonable. Indeed, the scatter is reduced and data are closer to a single curve. During the falling limb, the beds have a similar flow history and bed surface arrangement (verified with the scanner surveys). During the rising limb, differences are still present between the beds, even ignoring the bed form effect on flow resistance (Figure 11a). This could indicate that the hypothesis of similar bed roughness is inappropriate and that the estimation of τ_g with a single bed roughness coefficient is probably mistaken. In addition, changes in bed arrangement may not influence only flow resistance, but also bed stability defined by the distributions of the dislodging forces, which individual grains can resist before moving (Tait, 1993). Bed stability is assessed by bed roughness and additional indicators such as the lengths of bedforms and structures, the degree of armoring (A_r) (Cooper and Tait, 2009) and the main orientation of the bed surface grains (Φ) (Friedrich, 2010). The analysis of the laser scanner surveys supports the hypothesis of an incorrect estimation of τ_g , but does not inform on the impact of bed arrangement on bed

Author-produced version of the article published in Earth Surface Processes and Landforms , 2018
The original publication is available at https://onlinelibrary.wiley.com/doi/abs/10.1002/esp.4322
doi : 10.1002/esp.4322

stability.

In bedload prediction models, flow resistance and bed mobility are often represented using hydraulic roughness (k_s) and a criterion defining the gravel's incipient motion (τ^*_{ref}), respectively (Wilcock et al., 2009). Improving these models requires assessing changes in both flow resistance and bed stability. Regarding the experimental results reported herein, both τ^*_{ref} and k_s seem sensitive to change in bed arrangement. They are therefore at least dependent on a combination of several indicators of bed surface arrangement, e.g. $k_s = f(\sigma_{zg}, \Delta_{x0}, \Delta_{y0}, A_r, \Phi, ...)$ and $\tau^*_{\mathrm{ref}} = f(\sigma_{zg}, \Delta_{x0}, \Delta_{y0}, A_r, \Phi, ...)$.

We were not able to explain the link between q_s and bed arrangement parameters exhaustively, nor to reduce the number of controlling parameters. For this to be achieved, supplementary data are needed. Nevertheless, some correlations were found between τ^*_{ref} and bed surface indicators, helping to understand the impact of bed arrangement on bedload transport, such as the correlation between the decrease in τ^*_{ref} and the decrease in geometrical grain roughness, the correlation between the increase in τ^*_{ref} and the increase in bedform heights, structure lengths and bed armoring degree, the correlation between the increase in τ^*_{ref} and the appearance of a preferential grain orientation. Figure 12 illustrates some of these observed correlations.

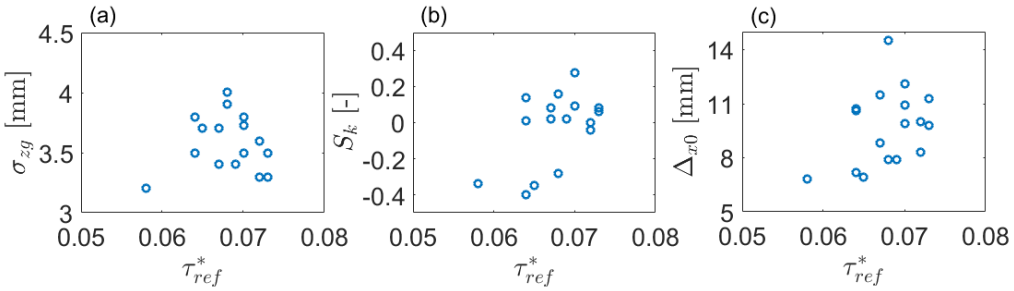

Figure 12: Relation between dimensionless reference bed shear stresses and their associated bed surface indicators. Bed surface parameters are (a) geometrical grain roughness or (b) bed armoring degree or (c) the length of the bed surface structures in the flow direction.

Author-produced version of the article published in Earth Surface Processes and Landforms , 2018
The original publication is available at https://onlinelibrary.wiley.com/doi/abs/10.1002/esp.4322
doi : 10.1002/esp.4322

Impact of geotechnical bed properties

Our observations revealed that the presence of infiltrated fine sediments needs to be taken into account when studying bedload dynamics.

Tests were performed on beds infiltrated from the bottom up with fine sediments having similar grain sizes but different geotechnical properties (H-G/FS and H-G/Ms). The results showed that fine sediments affected gravel mobility differently. In presence of Ms, q_s was reduced, whereas in presence of FS, q_s was enhanced for similar bed shear stress. The size of the fines is therefore not the only parameter to be considered when studying infiltrated beds. The geotechnical properties of the gravel matrix can change depending on the type of infiltrated fine sediments (Table 1). Bed permeability, consolidation and fine sediment shape are also important parameters controlling q_s.

Bed permeability k mainly depends on the grain size and particle shape of the coarse and fine particles. Previous studies highlighted the impact of bed permeability on hydraulic roughness (Manes et al., 2009; Hamm et al., 2011). Hamm et al. (2011) measured bed shear stresses in open-channel flows over permeable beds formed by glass beads ($D_{50} = 1.5\,\mathrm{mm}$) or cobbles ($D_{50} \approx 6.5\,\mathrm{cm}$). They found that bed shear stresses were 1.5 - 2 times greater than those for impermeable beds under equivalent hydraulic conditions. This effect was attributed to the momentum balance associated with water exchange across the sediment-water interface (Manes et al., 2009). This increase in bed shear stress facilitates sediment movement for permeable beds. In permeable beds, the bed shear stress is distributed over a finite depth instead of a surface as in an impermeable bed. The observation of the in-bed water velocity profile suggests that this depth is limited to one or two grain diameters and that most of the shear stress is applied on grains of the first bed surface layer (Leonardson, 2010). In impermeable beds, the bed shear stress acts predominantly on the upper part of the surface grain, whereas in the case of permeable beds, it acts on the whole grain, therefore enhancing grain motion. In our case, beds infiltrated with fine sediments from the bottom up have similar bed permeabilities, which are much

smaller than in the case of L-G beds (Table 1). Permeability Reynolds numbers ($Re_k = \sqrt{k}u^*/\nu$) are less than 1, indicating that these beds will behave as if they were impermeable (Breugem et al., 2006; Manes et al., 2009). On the contrary, L-G beds are considered as permeable beds (high values of Re_k). Gravel mobility should be reduced on H-G/Ms and H-G/FS beds compared to L-G beds. However, Figure 8 shows that this was not always the case. If L-G beds (permeable) were put into motion more easily than H-G/Ms beds (impermeable), the opposite behavior during the falling limb was observed between L-G beds (permeable) and H-G/FS beds (impermeable). Therefore, other factors than bed permeability may also control the bedload rate.

The decreased erodibility of a H-G/Ms bed can be attributed to a change in bed stability due to the higher consolidation caused by the presence of fine sediments (see C_u in Table 1). The H-G/FS bed was not consolidated ($C_u = 0$) compared to beds formed with Ms. The latter consolidates the gravel matrix and prevents gravel from moving. It is important to recall that C_u increases with the decrease in water content within the bed, which depends on the residence time of fine sediments. This residence time (T_r) corresponds to the time during which the fines were present in the drained gravel matrix before the beginning of the sediment transport experiment (see Figure 4, the time between steps (3b) and (4)). The longer this time is, the less erodible the bed material is. Indeed, H-G/Ms beds with the longest T_r are those with the lowest bedload rate (T_r equal 12, 5 and 3 days for H-G/Ms-5, H-G/Ms-6 and H-G/Ms-9, respectively) (Figure 8). In this way, q_s decreases as bed material consolidation increases. The hysteresis pattern of H-G/Ms-5 showed a clockwise loop as opposed to the other tests performed with Ms. This difference can be explained by remarkably high bed consolidation. During the rising limb, the flow removed fines from the first surface layer, while transporting some gravel particles. Then the flow encountered strongly consolidated fine sediments located on the subsurface where gravel is totally enclosed by Ms. Fine sediments present on the bed surface were easier to de-clog than those present in the subsurface. That is why a reduction in the

bedload rate occurred during the falling limb of the hydrograph. The residence time of fine sediments T_r appears to be an important parameter for predicting bedload rate.

The difference in bedload rate between the H-G/Ms and H-G/FS bed experiments may also be related to the shape of fine sediments. Several authors have investigated the effect of coarse sediment shape on bed shear stress (Li and Komar, 1986; Durafour et al., 2015). They found that particles with non-spherical shapes (flat, angular or elongated) have stronger imbrication patterns than spherical particles. Li and Komar (1986) showed that the bed shear stress required to put into motion non-spherical material might be up to six times greater than the bed shear stress for moving spherical grains. Durafour et al. (2015) observed that changes in bed shear stress were controlled by changes in the sediment circularity index (C_I). Transposing these findings for coarse particles to fine particles used in this study could explain why H-G/FS beds were easier to move than H-G/Ms beds. Ms particles ($C_I = 0.75$) contribute to consolidating the bed because of their angular and elongated shapes, reducing the sediment transport in contrast to spherical FS particles ($C_I = 0.99$) (Table 1). The significant dispersion of the GSD of the medium silt (Figure 2) probably also reduces the porosity and enhances the bed consolidation. The increase in erodibility of the H-G/FS bed may be attributed to a decrease in bed stability due to the lubrication effect of the circular FS washed out of the gravel matrix.

Importance of fine sediment concentration

Tests were performed on beds infiltrated with non-cohesive fine sediments having different grain sizes (H-G/FS and H-G/S). In both cases, the gravel mobility was enhanced, but to a lesser extent in the H-G/FS experiment.

Previous studies showed that gravel transport increased in presence of non-cohesive fine sediments within the bed (Jackson and Beschta, 1984; Wilcock et al., 2001; Curran, 2007; Koll and Dittrich, 2010). This increase is often associated with

a reduction of the mean grain diameter characterizing the overall bed (Hill et al., 2017). In our case, the bedload rate was higher in the presence of sand than in the presence of fine sand. Yet, the mean grain diameter of the bed was lower for the H-G/FS bed than for the H-G/S bed. Therefore, previous indicators might not be suitable for characterizing gravel transport with infiltrated beds.

In the H-G/FS experiment, gravel transport was not influenced by fine sediments during the rising limb (the results were similar to those found during the falling limb of the L-G experiments), whereas it increased during the falling limb (Figure 8). Yet, we expect the GSD of the overall bed surface to increase as part of the fines are washed out. The increase in sediment transport might be explained by the fact that between the rising and falling limbs, the fine sediment concentration within the flow increased due to the re-suspension of fine particles. In their experiments, Wilcock and Crowe (2003) found that high fine sediment content in the surface ($> 30\,\%$) strongly enhances bedload rate. Considering the H-G/FS results, we believe that fine sediment concentration in the bedload layer c_f (and not in the surface) is a controlling parameter for gravel transport. We define the bedload layer as the thin layer at the bed surface, where gravel particles are transported and where interactions between fine and coarse sediments occur. The analysis of c_f can also explain the difference between the H-G/FS and H-G/S experiments. Indeed, for the H-G/S experiment, sand moves as bedload resulting in a much higher concentration in sand within this layer than for the H-G/FS experiment (FS was transported in suspension). c_f depends on the transport mode (bedload or suspension) and bedload rates are higher for higher c_f such as in the H-G/S experiment. The H-G/S test also highlights the importance of considering the time variation of c_f when studying gravel transport. Knowing the fine sediment distribution within the bed (related to the type of infiltration) helps predict the temporal evolution of c_f. We suggest taking $c_f(t)$ into account in new bedload models.

Author-produced version of the article published in Earth Surface Processes and Landforms , 2018
The original publication is available at https://onlinelibrary.wiley.com/doi/abs/10.1002/esp.4322
doi : 10.1002/esp.4322

Recommendations for bedload prediction

Based on our experiments (Figure 10) and on previous studies (Wilcock and Crowe, 2003; Hassan et al., 2006; Jain and Kothyari, 2009; Recking, 2009), a methodology for improving bedload prediction in gravel-bed rivers is suggested. In this paper, we provide clues for estimating τ^*_{ref} more accurately, which is a key parameter in bedload models. Adjusting the τ^*_{ref} value according to the bed arrangement and gravel matrix composition is the base of the methodology. The methodology for predicting the bedload rate of a specific gravel-bed typically depends on the bedload model used, and more specifically on the definition of τ^*_{ref} in the model.

The methodology can be recapped as follows:

1. Make a first estimate of τ^*_{ref} as a function of the chosen bedload formula (e.g. Meyer-Peter and Müller, 1948) and assume that it corresponds to τ^*_{ref} for loose gravel beds. For example, if τ^*_{ref} is assumed equal to the critical dimensionless bed shear stress τ^*_{cr} defined by Shields (1936), one can use the gravel GSD characteristics and existing diagrams or equations (Yalin and Karahan, 1979; Soulsby and Whitehouse, 1997) to calculate its value.

2. Characterize the gravel-bed (i.e., level of bed arrangement, degree of clogging and type of bed infiltration).

3. Adjust τ^*_{ref} according to bed configuration (from 0 to +12 % according to the level of arrangement, from 0 to +12 % according to the level of consolidation and from -40 to 0 % according to the concentration of non-cohesive fine sediments in the bedload layer). These values are given as an indication and are based on our laboratory results (Figure 6 and 8). They were calculated using the percentage difference of τ^*_{ref} between experiments from the same couple of experiments. An average is then made for each type of beds. The percentage difference can slightly increase if the arbitrary value for $q_{s\text{-ref}}$ is chosen smaller. However, the trends (i.e. increasing or decreasing τ^*_{ref}) remain the same.

4. Compute q_s using the new τ^*_{ref} and the related bedload formula.

Author-produced version of the article published in Earth Surface Processes and Landforms , 2018
The original publication is available at https://onlinelibrary.wiley.com/doi/abs/10.1002/esp.4322
doi : 10.1002/esp.4322

We do not claim that the above methodology provides quantitative values for τ^*_{ref}. Even if the first estimate of τ^*_{ref} is mistaken, the recommended relative adjustment should still be valid and coherent. Further studies with different sediments and hydraulic conditions should be tested to validate the given qualitative ranges of adjustment. The final bedload trends are in coherence with those found in previous studies, namely a decrease in q_s with strong bed arrangement (Hassan et al., 2006; Guney et al., 2013) and in presence of cohesive fine sediments (Jain and Kothyari, 2009; Barzilai et al., 2013) and an increase in q_s in presence of non-cohesive fine sediments (Wilcock and Crowe, 2003; Curran and Wilcock, 2005). In-situ tests were conducted to verify this methodology (Camenen et al., 2015).

Even if the slope effect was not studied in this paper, it could be interesting to suggest an adjustment as a function of changes in bed slope. Previous studies found that τ^*_{ref} increases with an increase in bed slope (Chiew and Parker, 1994; Shvidchenko and Pender, 2000; Mueller et al., 2005; Lamb et al., 2008; Recking, 2009). The bedload rate is then lower at high slopes. The reasons for this decrease remain only partially explored. In steep flows, the relative roughness (k_s/h) is high and the bed arrangement is strong. Changes in relative roughness impact the flow structure and turbulence, modifying the bedload rate. The slope effect is actually a consequence of the linked effects of bed arrangement (Shvidchenko and Pender, 2000) and relative roughness (Lamb et al., 2008; Recking, 2009) that should be taken into account when predicting the bedload rate.

Conclusion

Original laboratory experiments were conducted to investigate the mobility of gravel under low bed shear stresses. Particular attention was paid to the roles played by the gravel surface arrangement and by fine sediments infiltrating the gravel matrix. A total of 15 experiments were conducted with different bed configurations: clean loose and packed gravel beds, and gravel beds infiltrated with sand, non-cohesive fine sand or cohesive medium silt. Unsteady flow conditions ensuring low bed shear

stresses were simulated. Laser scanning of the bed topography was performed to retrieve information on bed changes. The results showed that both the bed arrangement (e.g., structure sizes, degree of bed armoring, surface grain imbrication and orientation) and the presence of fine sediments (e.g., nature, shape and concentration of fines, degree of bed consolidation) significantly govern the transport of gravel.

The bedload rate decreases with decreasing bed roughness, increasing grain structure lengths, increasing grain imbrication and with gravel particles preferentially aligned with the flow direction. The mobility of a packed gravel bed decreases up to 12 % compared to a loose gravel bed. Cohesive and angular silt infiltrated into the gravel matrix strongly reduces the bedload rate by consolidating the gravel bed, thereby increasing the reference bed shear stress up to 12 % compared to a clean gravel bed. The opposite behavior was observed with non-cohesive and spherical fine particles, namely gravel bed lubrication due to fine presence and a reduction of the reference bed shear stress up to 40 % compared to a clean gravel bed. Under low-flows, the gravel movement can be enhanced if the concentration of fine particles is high enough in the bedload layer, which is accompanied by a reduction in flow roughness and turbulence and an acceleration in near-bed flow.

We suggest a methodology for improving the computation of bedload rate in mountain rivers. We recommend adjusting the dimensionless reference bed shear stress in bedload transport capacity formulae according to the degree of bed surface arrangement (loose or packed), the presence of fines (concentration in the bedload layer) and the characteristics of fines infiltrated into the bed (cohesive or non-cohesive, grain shape): from 0 % to +12 % depending on the degree of bed arrangement, from 0 % to +12 % for gravel infiltrated with cohesive and angular fine particles, and from -40 % to 0 % for gravel infiltrated with non-cohesive fine particles.

The present work is an additional step toward a consistent investigation of gravel transport in open channels. Further experiments could help build a new bedload

model that considers the effect of bed arrangement and gravel matrix composition. Tests could be conducted under a broader range of flow conditions (e.g., flow hydrographs, changing flow directions), channel geometry (e.g., bed slope) and more complex configurations (e.g., water-worked bed, alternate bars), with various bed material compositions (e.g., gravel infiltrated with silt/sand mix).

Acknowledgements

The experiments were supported by Irstea, EDF (Electricité de France), the French Water Agency (AE-RMC) and the OSR research program (Rhône Sediment Observatory). The Irstea Lyon-Villeurbanne metrology team, especially Alexis Buffet, are gratefully acknowledged for their technical support in performing the laboratory experiments. The authors would like to thank Sylvie Nicaise (Irstea Aix-en-Provence) and Khedidja Abbaci (Irstea Lyon-Villeurbanne) for their assistance in the characterization of sediment properties.

References

Ancey, C., Bohorquez, P., and Heyman, J. (2015). Stochastic interpretation of the advection-diffusion equation and its relevance to bed load transport. *Journal of Geophysical Research: Earth Surface*, 120(12):2529–2551. 2014JF003421.

Barzilai, R., Laronne, J. B., and Reid, I. (2013). Effect of changes in fine-grained matrix on bedload sediment transport in a gravel-bed river. *Earth Surface Processes and Landforms*, 38:441–448.

Beschta, R. L. and Jackson., W. L. (1979). The intrusion of sediments into a stable gravel bed. *Journal of the Fisheries Research Board of Canada*, 36(2):204–210.

Breugem, W., Boersma, B., and Uittenbogaard, R. (2006). The influence of wall permeability on turbulent channel flow. *Journal of Fluid Mechanics*, 562:35–72.

783 Buffington, J. M. and Montgomery, D. R. (1997). A systematic analysis of eight
784 decades of incipient motion studies, with special reference to gravel-bedded rivers.
785 *Water Resources Research*, 33(8):1993–2029.

786 Camenen, B., Herrero, A., Dramais, G., Thollet, F., Le Bescond, C., Perret, E., and
787 Berni, C. (2015). Field experiment on the dynamics of fine and coarse sediments
788 over a gravel bar in an alpine river. In *Proc. 36th IAHR Congress*, The Hague,
789 The Netherlands.

790 Camenen, B. and Larson, M. (2005). A general formula for non-cohesive bed load
791 transport. *Estuarine, Coastal and Shelf Science*, 63:246–260.

792 Camenen, B., Le Coz, J., Paquier, A., and Lagouy, M. (2010). An estimation
793 of gravel mobility over an alpine river gravel bar (Arc en Maurienne, France)
794 using PIT-tag tracers. In Dittrich, A., Koll, K., Aberle, J., and Geisenhainer,
795 P., editors, *River Flow, Proc. 5th International Conference on Fluvial Hydraulics*,
796 pages 953–960, Braunschweig, Germany.

797 Chiew, Y.-M. and Parker, G. (1994). Incipient sediment motion on non-horizontal
798 slopes. *Journal of Hydraulic Research*, 32:649–660.

799 Church, M., Hassan, M. A., and Wolcott, J. F. (1998). Stabilizing self-organized
800 structures in gravel-bed stream channels: Field and experimental observations.
801 *Water Resources Research*, 34(11):3169–3179.

802 Cooper, J. R. and Tait, S. J. (2009). Water-worked gravel beds in laboratory flumes
803 - a natural analogue ? *Earth Surface Processes and Landforms*, 34(3):384–397.

804 Cui, Y., Wooster, J. K., Baker, P. F., Dusterhoff, S. R., Sklar, L. S., and Dietrich,
805 W. E. (2008). Theory of fine sediment infiltration into immobile gravel bed.
806 *Journal of Hydraulic Engineering*, 134(10):1421–1429.

807 Curran, J. and Wilcock, P. R. (2005). Effect of sand supply on transport rates in a
808 gravel-bed channel. *Journal of Hydraulic Engineering*, 131(11).

809 Curran, J. C. (2007). The decrease in shear stress and increase in transport rates
810 subsequent to an increase in sand supply to a gravel-bed channel. *Sedimentary*
811 *Geology*, 202(3):572–580. Special issue: From Particle Size to Sediment Dynamics.

812 Curran, J. C. (2010). An investigation of bed armoring process and the formation
813 of microclusters. In *2nd Joint Federal Interagency Conference*, Las Vegas, NV.

814 Durafour, M., Jarno, A., Le Bot, S., Lafite, R., and Marin, F. (2015). Bedload trans-
815 port for heterogeneous sediments. *Environmental Fluid Mechanics*, 15(4):731–751.

816 Einstein, H. A. (1968). Deposition of suspended particles in a gravel bed. *Journal*
817 *of Hydraulic Division*, 94(5):1197–1204.

818 Friedrich, H. (2010). Evaluation of statistical analysis techniques for developing
819 bedforms recorded in 3d. Master's thesis, The Departement of Civil and Environ-
820 mental Engineering, the University of Auckland., New Zealand.

821 Frostick, L. E., Lukas, P. M., and Reid, I. (1984). The infiltration of fine matri-
822 ces into coarse-grained alluvial sediments and its implications for stratigraphical
823 interpretation. *Journal of the Geological Society*, 141:955–965.

824 Gibson, S., Abraham, D., Heath, R., and Schoellhamer, D. (2009). Vertical grada-
825 tional variability of fines deposited in a gravel framework. *Sedimentology*, 56:661–
826 676.

827 Gibson, S., Abraham, D., Ronald, H., and Schoellhamer, D. (2010). Bridging process
828 threshold for sediment infiltrating into a coarse substrate. *Journal of Geotechnical*
829 *and Geoenvironmental Engineering*, 136(2).

830 Guney, M. S., G., B., and Aksoy, A. (2013). Experimental study of the coarse
831 surface development effect on the bimodal bed-load transport under unsteady
832 flow conditions. *Journal of Hydraulic Engineering*, 139(1).

833 Hamm, N. T., Dade, W. B., and Renshaw, C. E. (2011). Fine particle deposition to
834 porous beds. *Water Resources Research*, 47(W11508):1–13.

Hassan, M. A. and Church, M. (2000). Experiments on surface structure and partial sediment transport on a gravel bed. *Water Resources Research*, 36(7):1885–1895.

Hassan, M. A., Egozi, R., and Parker, G. (2006). Experiments on the effect of hydrograph characteristics on vertical grain sorting in gravel bed rivers. *Water Resources Research*, 42(9).

Haynes, H., Vignaga, E., and Holmes, W. M. (2009). Using magnetic resonance imaging for experimental analysis of fine-sediment infiltration into gravel beds. *Sedimentology*, 56(7):1961–1975.

Herrero, A. and Berni, C. (2016). Sand infiltration into a gravel bed: A mathematical model. *Water Resources Research*, 52(11):8956–8969.

Hill, K., Gaffney, J., Baumgardner, S., Wilcock, P., and Paola, C. (2017). Experimental study of the effect of grain sizes in bimodal mixture on bed slope, bed texture, and the transition to washload. *Water Resources Research*, 53:923–941.

Hodge, R., Sear, D., and Leyland, J. (2013). Spatial variations in surface sediment structure in riffle-pool sequences: a preliminary test of the Differential Sediment Entrainment Hypothesis (DSEH). *Earth Surface Processes and Landforms*, 38:449–465.

Ikeda, H. and Iseya, F. (1988). Experimental study of heterogeneous sediment transport. Technical Report 12, Environmental Reserch Center, University of Tsukuba. 50p.

Jackson, W. L. and Beschta, R. L. (1984). Influences of increased sand delivery on the morphology of sand and gravel channel. *Journal - American Water Works Association*, 20(4):527–533.

Jain, R. K. and Kothyari, U. C. (2009). Cohesion influences on erosion and bed load transport. *Water Resources Research*, 45.

Koll, K. and Dittrich, A. (2010). Sediment transport over a static armour layer and its impact on bed stability. In Dittrich, A., Koll, K., Aberle, J., and Geisenhainer, P., editors, *River Flow, Proc. 5th International Conference on Fluvial Hydraulics*, pages 929–936, Braunschweig, Germany.

Kondolf, G. M. and Wolman, M. G. (1993). The sizes of salmonid spawning gravel. *Water Resources Research*, 29:2275–2285.

Kothyari, U. C. and Jain, R. K. (2008). Influence of cohesion on the incipient motion condition of sediment mixtures. *Water Resources Research*, 44(W04410).

Krishnappan, B. G. and Engel, P. (2006). Entrapment of fines in coarse sediment beds. In *River Flow, Proc. 3rd International Conference on Fluvial Hydraulics*, Lisbon, Portugal. Taylor & Francis.

Lamb, M. P., Dietrich, W. E., and Venditti, J. G. (2008). Is the critical shields stress for incipient sediment motion dependent on channel-bed slope? *Journal of Geophysical Research*, 113(F02008):20 p.

Leonardson, R. (2010). *Exchange of fine sediments with gravel riverbeds*. Phd thesis, Berkeley University, Berkeley, California, USA.

Li, Z. and Komar, P. D. (1986). Laboratory measurements of pivoting angle for applications to selective entrainment of gravel in a current. *Sedimentology*, 33(3):413–423.

Lisle, T. E. (1989). Sediment transport and resulting deposition in spawning gravels, North Coastal California. *Water Resources Research*, 25(6):1303–1319.

Manes, C., Pokrajac, D., McEwan, I., and Nikora, V. (2009). Turbulence structure of open channel flows over permeable and impermeable beds: A comparative study. *Physics of Fluids*, 21(12):125109.

Mao, L. (2012). The effect of hydrographs on bed load transport and bed sediment spatial arrangement. *Journal of Geophysical Research: Earth Surface*, 117(F3).

Mao, L., Cooper, J. R., and Frostick, L. E. (2011). Grain size and totopographic differences between static and mobile armour layers. *Earth Surface Processes and Landforms*, 36:1321–1334.

Marion, A., Tait, S. J., and McEwan, I. K. (2003). Analysis of small-scale gravel bed topography during armoring. *Water Resources Research*, 39(12-1334):1–11.

Marquis, G. A. and Roy, A. G. (2012). Using multiple bed load measurements: toward the identification of the bed dilation and contraction in gravel-bed rivers. *Journal of Geophysical Research*, 117(F01014):1–16.

Meyer-Peter, E. and Müller, R. (1948). Formulas for bed-load transport. In *Proc. 2nd IAHR Congress*, pages 39–64, Stockholm, Sweden.

Mueller, E. R., Pitlick, J., and Nelson, J. M. (2005). Variation in the reference shields stress for bed load transport in gravel-bed streams and rivers. *Water Resources Research*, 41(W04006):1–10.

NF P 94-072 (1995). Sols: reconnaissance et essais. essai scissométrique en laboratoire. Technical report, AFNOR Norm.

Nikora, V. I., Goring, D. G., and Biggs, B. J. F. (1998). On gravel-bed roughness characterization. *Water Resources Research*, 34(3):517–527.

Nuñez Gonzalez, F. (2016). Infiltration of fine sediment mixtures through poorly sorted immobile coarse beds. *Water Resources Research*, 52(12):9306–9324.

Parker, G. (2008). *Sediment Engineering - Processes, Measurements, Modeling, and Practice (Editor: M.H. Garcia)*, chapter Transport of gravel and sediment mixtures, pages 165–252. American Society of Civil Engineers.

Parker, G., Klingeman, P. C., and McLean, D. G. (1982). Bed load and size distribution in paved gravel-bed streams. *Journal of Hydraulics Division*, 108(HY4):544–571.

Perret, E., Berni, C., Herrero, A., Camenen, B., Buffet, A., and El kadi Abderrezzak, K. (2016). Laser scanning method to characterize bed arrangement and its influence on incipient motion of gravel sediments. In *River Flow, Proc. 8th International Conference on Fluvial Hydraulics*, St Louis, USA.

Petit, F., Houbrechts, G., Peeters, A., Hallot, E., Van Campenhout, J., and Denis, A.-C. (2015). Dimensionless critical shear stress in gravel-bed rivers. *Geomorphology*, 250:308–320.

Pitlick, J. and Van Steeter, M. M. (1998). Geomorphology and endangered fish habitats of the upper colorado river: 2. linking sediment transport to habitat maintenance. *Water Resources Research*, 34(2):303–316.

Proffitt, G. and Sutherland, A. (1983). Transport of non-uniform sediments. *Journal of Hydraulic Research*, 21(1):33–43.

Qin, J., Zhong, D., Wang, G., and Ng, S. L. (2012). On characterization of the imbrication of armored gravel surfaces. *Geomorphology*, 159-160:116–124.

Recking, A. (2009). Theoretical development on the effects of changing flow hydraulics on incipient bedload motion. *Water Resources Research*, 45:1–16.

Recking, A., Libault, F., Peteuil, C., and Jolimet, T. (2012). Testing bedload transport equations with consideration of time scales. *Earth Surface Processes and Landforms*, 37(7):774–789.

Recking, A., Liébault, F., Peteuil, C., and Jolimet, T. (2012). Testing bedload transport equations with consideration of time scales. *Earth Surface Processes and Landforms*, 37:774–789.

Reid, I., Frostick, L. E., and Layman, J. T. (1985). The incidence and nature of bedload transport during flood flows in coarse-grained alluvial channels. *Earth Surface Processes and Landforms*, 10:33–44.

936 Sakthivadivel, R. and Einstein, H. A. (1970). Clogging of porous column of spheres
937 by sediment. *Journal of the Hydraulics Division*, 96(2):461–472.

938 Schälchli, U. (1992). The clogging of coarse gravel river beds by fine sediment.
939 *Hydrobiologia*, 235-236(1):189–197.

940 Sear, D. A. (1993). Fine sediment infiltration into gravel spawning beds within a reg-
941 ulated river experiencing floods: ecological implications for salmonids. *Regulated*
942 *Rivers: Research and Management*, 8:373–390.

943 Shields, A. (1936). Anwendung der Ahnlichkeits-mechanik und der turbulenz-
944 forschung auf die geshiebebewegung. *Preussische Versuchsanstalt fur Wasserbau*
945 *und Schiffbau*, 26:26 p. Berlin, Germany.

946 Shvidchenko, A. B. and Pender, G. (2000). Flume study of the effect of relative
947 depth on the incipient motion of coarse uniform sediments. *Water Resources*
948 *Research*, 36(2):619–628.

949 Smart, G. M., Maurice, M. J., and Walsh, J. M. (2002). Relatively rough flow
950 resistance equations. *Journal of Hydraulic Engineering*, 128(6):568–578.

951 Soulsby, R. L. (1997). *Dynamics of marine sands, a manual for practical applica-*
952 *tions*. Thomas Telford, London, UK. ISBN 0-7277-2584 X.

953 Soulsby, R. L. and Whitehouse, R. J. S. W. (1997). Threshold of sediment motion in
954 coastal environment. In *Proc. Pacific Coasts and Ports'97 Conf.*, pages 149–154,
955 Christchurch, New Zealand. University of Canterbury.

956 Tait, S. (1993). *The physical processes of bed armouring in mixed grain sediment*
957 *transport*. PhD thesis.

958 USWES (1935). Studies of river bed materials and their movement with special
959 reference to the lower Mississippi River. Technical Report 17, U. S. Army Corps
960 of Engineers, Vicksburg, Mississippi, U. S. A. 161 pp.

961 Vanoni, V. A. and Brooks, N. H. (1957). Laboratory studies of the roughness
962 and suspended load of alluvial streams. Technical report, Sedimentation Lab. ,
963 California Institute of Technology, Pasadena, California, USA.

964 Voepel, H., Ahmed, S., Hodge, R., Leyland, J., and Sear, D. (2017). Variations
965 in grain-scale sediment structure and entrainment force in a gravel-bed channel
966 as a function of fine sediment content and morphological location. In *European*
967 *Geophysical Union*, Vienna.

968 Wainwright, J., Parsons, A. J., Cooper, J. R., Gao, P., Gillies, J. A., Mao, L.,
969 Orford, J. D., and Knight, P. G. (2015). The concept of transport capacity in
970 geomorphology. *Reviews of Geophysics*, 53.

971 Wharton, G., Mohajeri, S., and Righetti, M. (2017). The pernicious problem of
972 streambed colmation: a multi-disciplinarity reflection on the mechanisms, causes,
973 impacts, and management challenges. *Wiley Interdisciplinary Reviews: Water*,
974 4:1–17.

975 Wilcock, P., Potlick, J., and Cui, Y. (2009). Sediment transport primer: estimating
976 bed-material transport in gravel-bed rivers. Technical report, U. S. Department
977 of Agriculture, Forest Service, Rocky Mountain Research Station.

978 Wilcock, P. R. (2001). Toward a practical method for estimating sediment transport
979 rates in gravel-bed rivers. *Earth Surface Processes and Landforms*, 26:1395–1408.

980 Wilcock, P. R. and Crowe, J. C. (2003). Surface-based transport model for mixed-
981 size sediment. *Journal of Hydraulic Engineering*, 129(2):120–128.

982 Wilcock, P. R. and Kenworthy, S. T. (2002). A two-fraction model for the transport
983 of sand/gravel mixtures. *Water Resources Research*, 38(10):1194.

984 Wilcock, P. R., Kenworthy, S. T., and Crowe, J. C. (2001). Experimental study of
985 the transport of mixed sand and gravel. *Water Resources Research*, 37:3349–3358.

Wilcock, P. R. and McArdell, B. W. (1993). Surface-based fractional transport rates: Mobilization thresholds and partial transport of a sand-gravel sediment. *Water Resources Research*, 29(4):1297–1312.

Wren, D. G., Langendoen, E. J., and Kuhnle, R. A. (2011). Effects of sand addition on turbulent flow over an immobile gravel bed. *Journal of Geophysical Research: Earth Surface*, 116(F1).

XP CEN ISO/TS 17892-6 (2006). Reconnaissance et essais géotechniques - essais de laboratoire sur les sols - partie 6 : essai de pénétration de cône. Technical report, AFNOR norms.

Yalin, M. and Karahan, E. (1979). Inception of sediment transport. *Journal of Hydraulic Engineering*, 105:1433–1443.

Table 1: Main geometrical and geotechnical characteristics of the sediments or mixtures used in this study.

Sediments	D_{50}, d_{50} (mm)	σ_g (-)	w_s (mm/s)	C_I (-)	p (-)	k (m^2)	$C_{u\text{-sat}}$ (kPa)	$C_{u\text{-20-30\%}}$ (kPa)	Re_k (-)
G	6.8	1.3	340	0.84	0.42	$3.6.10^{-8}$	0	0	15.7
S	0.813	1.34	110	0.84	NE	NE	0	0	NE
FS	0.066	1.3	3.6	0.99	0.4	$3.4.10^{-12}$	0	11-12	0.15
MS	0.04	2.5	1.3	0.75	0.56	$3.4.10^{-12}$	2.4-28	250-500	0.15
Mixtures									
G/FS	NE	NE	NA	NA	0.17	$1.9.10^{-11}$	NE	NE	0.36
G/Ms	NE	NE	NA	NA	0.23	$6.7.10^{-11}$	NE	NE	0.68

D_{50} and d_{50} are the median grain diameters of the coarse and fine sediments, respectively [mm]; σ_g is the geometric standard deviation of the GSD; w_s is the settling velocity computed using Soulsby (1997) equation; CI is the circularity index; p is the bed porosity; Mixture porosity were calculated using the comparison between gravel porosity and the maximum fine content that can contain the gravel matrix as presented in Leonardson (2010). k is the bed permeability computed with the Kozeny-Carman relation; $C_{u\text{-sat}}$ is the bed consolidation measured for water-saturated beds; $C_{u\text{-20-30\%}}$ is the bed consolidation measured when the bed water content is about 20-30 %; $Re_k = \sqrt{k}u^*/\nu$ is the permeability Reynold number; $u^* = \sqrt{ghI}$ is calculated for a standard case where $I = 0.01$ and $h = 0.07$ m. NE and NA refer to not evaluated and not applicable data, respectively.